Asymptotic behavior of radially symmetric self-focused beams

F. Vidal and T. W. Johnston
Institut National de la Recherche Scientifique-Énergie et Matériaux, 1650 Boulevard Lionel-Boulet, Case Postale 1020, Varennes, Québec, Canada J3X 1S2
(Received 5 August 1996)

Radially symmetric self-focused beams near solitonlike solutions are studied in the framework of the nonlinear Schrödinger equation for physically relevant nonlinearities. From the numerical solutions, three main types of oscillations are identified, which are characterized by one or more well-defined frequencies and by the presence or lack of the damping associated with radiation emission. Concepts borrowed from linear quantum mechanics are shown to provide many valuable insights into the observed behavior. [S1063-651X(97)00303-6]

PACS number(s): 03.40.Kf, 42.65.Jx, 52.35.Mw, 03.65.Ge

I. INTRODUCTION

When the envelope $u(\mathbf{r},t)$ of the electric field

$$\mathbf{E}(\mathbf{r},t)=\frac{1}{2}\hat{\mathbf{e}}\ u(\mathbf{r},t)\exp[i(\omega_0 t-k_0 z)]+\text{c.c.}$$

varies slowly in time t and along the propagation axis z and when the polarization of the electric field can be neglected [1], one obtains the parabolic approximation to the Maxwell wave equation, which, in a frame of reference moving at the velocity c^2k_0/ω_0, is

$$2i\omega_0\frac{\partial}{\partial t}u+c^2\nabla_\perp^2 u+\omega_0^2\delta\epsilon(\mathbf{r},t)u=0. \tag{1}$$

Here $\delta\epsilon(\mathbf{r},t)$ is the local variation of the medium's dielectric function and $\nabla_\perp^2$ is the transverse Laplacian. For media where $\delta\epsilon(\mathbf{r},t)$ depends on the local intensity of light, one obtains the nonlinear Schrödinger equation (NLSE) which is in its normalized form

$$i\frac{\partial}{\partial t}u+\nabla_\perp^2 u+f(|u|^2)u=0. \tag{2}$$

The scaled variables appearing in Eq. (2) are related to the physical ones in a manner that depends on the specific parameters determining the nonlinear function $\delta\epsilon(\mathbf{r},t)$. Equation (1) or (2) constitutes a widely used starting point for the modeling of the propagation of light beams in nonlinear media (see, for instance, [1–10]). It is therefore important to know and understand the general features of the solutions of Eq. (2) for physically relevant nonlinearities $f(|u|^2)$, a topic that is the main concern of this paper.

A well-known property of Eq. (2) is self-focusing: when $f(|u|^2)>0$ the nonlinearity acts locally as a focusing lens that can overcome diffraction. The beam can self-focus as a whole (whole beam self-focusing) or, when the beam power exceeds several times some critical value, the critical power, form several independent beamlets (filamentation) [11]. When self-focusing and diffraction equilibrate, Eq. (2) admits steady-state solutions [12], i.e., solitons.

In one spatial dimension, Eq. (2) with the simple Kerr nonlinearity $f(s)=s$, which yields the so-called cubic nonlinear Schrödinger equation (CNLSE), describes the propagation of light pulses in optic fibers [13] [the variables t and x are however interchanged in Eq. (2) in that case]. For this specific problem, Eq. (2) can be solved exactly by means of inverse scattering transforms [14]. It is known that for an arbitrary initial state the asymptotic or final state [i.e., in the notation of Eq. (2), for $t\to\infty$] is composed of a set of equilibrium states (solitons) and a certain amount of radiation, which means light that is not confined in the solitons and thus escapes to infinity. However, in two dimensions the solutions of the CNLSE are such that the self-focusing solutions will collapse, becoming singular at one or more points in a finite time [11,15], so that no equilibrium stable state exists. If the parabolic approximation in two dimensions remains valid (i.e., if large-angle diffraction [16] or large-angle frequency spreading [17] do not supervene) the nonlinearity must saturate, i.e., $f(s)<C$, where C is some positive number, in order to avoid this unphysical effect. The Kerr nonlinearity then appears as only the first term of the expansion of a saturable nonlinearity model as a function of the field amplitude. For usual saturable nonlinearities, Eq. (2) has no known analytical solutions (both in one and two dimensions) and one must mainly rely on numerical investigations.

In this paper we will consider specifically the algebraically saturable nonlinearity

$$f_A(s)=\frac{s}{1+s}, \tag{3}$$

which has recently been used to describe successfully the propagation of light in gas vapors [6–8] and can be justified from simple physical arguments. [Notice that the alternative form $as/(b+cs)$ on the right-hand side of Eq. (3), where a, b, and c are arbitrary nonzero constants, would add no more generality since it is always possible to normalize the field u, distances, and time in Eq. (2) so that f_A appears as in Eq. (3).] We have checked that the following discussion remains essentially the same for other (saturable) nonlinearities of physical interest, such as $f(s)=1-\exp(-s)$, which describes the slow ponderomotive self-focusing of laser beams in plasmas [1,3–5] and $f(s)=1-(1+s^2)^{-1/2}$, which de-

scribes self-focusing due to the relativistic increase of the electron mass [9,10] (independently of the electron displacement due to the ponderomotive force). Therefore, the nonlinearity (3) can be considered as typical of other physically relevant saturating nonlinearities.

Many important general results concerning the existence, uniqueness, and stability of the steady-state solutions of Eq. (2) for some saturable nonlinearities and for an arbitrary number of spatial transverse dimensions have been obtained [12]. However fewer general results are available for the time-dependent problem. For the CNLSE, analytical solutions have been constructed in one dimension, and for the approach to collapse in two dimensions [18]. For saturable nonlinearities useful results have also been obtained concerning the stability of the radially nonlinear excited states [19] and the growth rates of the filamentation process [10,20].

Recently, we have shown [21], from numerical investigations, that for large times the emerging beamlets in the filamentation process are all *very close* to different equilibrium states that can contain several times the critical power (up to 20 times has been observed). An upper bound on the total amount of power not confined in the final beamlets (radiation) has also been obtained. However, some questions remained unanswered about the fate of the beamlets so formed: Do they exactly reach equilibrium asymptotically, and if so, in what manner? It has long been known that for an arbitrarily chosen initial state the beam generally evolves in a very complicated way that is far from self-similar, even when radial [two-dimensional] symmetry is imposed (in which case only whole beam self-focusing of some fraction of the initial power is possible) [22]; however, the behavior of the self-focused beam near equilibrium is much simpler. This problem has been investigated analytically in Refs. [23,24] for the simplest saturable nonlinearity $f(s)=s-a^2s^2$ with a soft saturation, i.e., $a^2 \ll 1$, and for beams close to the critical power. It was concluded that in this particular context the beam behavior is, at least qualitatively, very similar to that of the well-known 1D CNLSE, i.e., the beam undergoes single-frequency small damped oscillations while emitting radiation and finally reaches an equilibrium state. In this paper we will show, from the numerical solutions of Eq. (2) in the radial case, that the asymptotic behavior of self-focused beams for the chosen physically relevant nonlinearity (3) presents a richer and more complex variety of behavior than that reported previously and that much of this observed behavior can be understood by means of concepts borrowed from elementary quantum mechanics.

In the next section we recall some general properties of the equilibrium solutions of the NLSE, Eq. (2). In Sec. III we present our numerical results about the behavior of the solutions near equilibrium. Section IV presents a discussion about the results of Sec. III from a quantum-mechanical point of view. Finally a summary and some concluding remarks are given in Sec. V.

II. EQUILIBRIUM SOLUTIONS

Equation (2) has equilibrium solutions of the form $u_\lambda(r,t)\equiv\phi_\lambda(r)\exp(i\lambda t)$, where $\phi_\lambda(r)$ satisfies the equation

$$\frac{1}{r}\frac{\partial}{\partial r}\left(r\frac{\partial}{\partial r}\phi_\lambda\right)+f(\phi_\lambda^2)\phi_\lambda-\lambda\phi_\lambda=0. \tag{4}$$

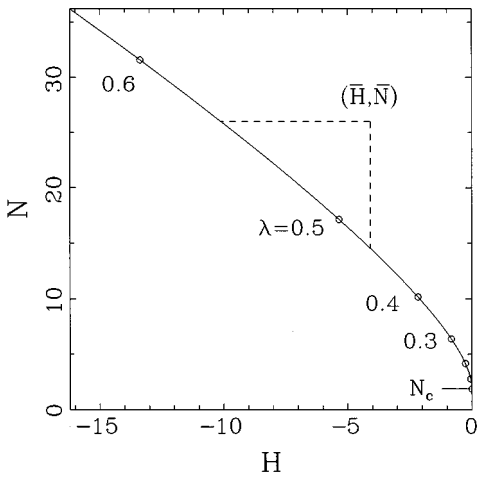

FIG. 1. Equilibrium locus in the plane N vs H. Small circles correspond to the values of λ from 0 to 0.6 by steps of 0.1. N_c is the critical value for N below which no equilibrium solution exists. The intersection point of the two dashed lines $(\bar{H},\bar{N})$ corresponds to some initial state of the beam.

We will be interested only in the purely radial monotonically decreasing solution (ground state) of Eq. (4) for a given λ, which we will denote $\phi_\lambda(r)$ with no special label. We choose the normalization so that $\phi_\lambda(r)$ is real. Equilibrium solutions of Eq. (4) can be represented in the N vs H plane [23], or H-N diagram, N and H being two well-known integrals of motion of Eq. (2), namely [12],

$$N[u]=(2\pi)^{-1}\int |u|^2 dx\, dy, \tag{5}$$

$$H[u]=(2\pi)^{-1}\int [|\nabla_\perp u|^2-\Phi(|u|^2)]dx\, dy, \tag{6}$$

where

$$\Phi(s)=\int_0^s f(\nu)d\nu. \tag{7}$$

Note that N (the notation is that dating from early soliton work) is proportional to the power of the light beam [25], which is conserved in absence of absorption, while H, which is the Hamiltonian associated with Eq. (4), seems to have no other simple physical significance. For the special case of nonlinearity we are considering, Eq. (3), one can see that equilibrium solutions exist only for $0<\lambda<1$ since $0\leqslant f_A\leqslant 1$. For this nonlinearity, ground-state solutions of Eq. (4) (i.e., radially monotonically decreasing functions) in two dimensions have been shown to be unique and stable [26]. The set of points (H_λ,N_λ), where $H_\lambda\equiv H[u_\lambda]$ and $N_\lambda\equiv N[u_\lambda]$, defines a locus in the N vs H plane [23] which is shown in Fig. 1 for the nonlinearity (3) in two dimensions. One can see that equilibrium solutions occur only (i) for $N\geqslant N_c$, where $N_c\approx 1.8623$ [as is always the case in two dimensions when $f(s)\to s$ as $s\to 0$], and (ii) for $H\leqslant 0$. One can show easily that Eq. (4) can be derived by minimizing the functional $H+\lambda N$ [23]. This has the important consequence that the representative point (H,N) of some function

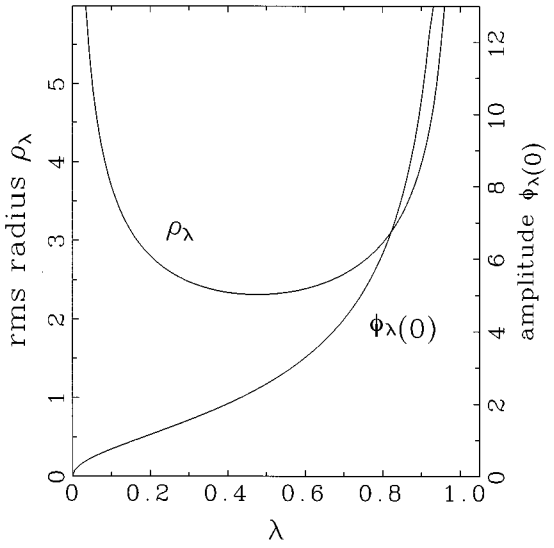

FIG. 2. Root-mean-square radius ρ_λ and maximum amplitude $\phi_\lambda(0)$ of the equilibrium ground-state solutions of Eq. (4) as a function of λ.

$u(\mathbf{r},t)$, in general different from any equilibrium solution $u_\lambda(r,t)$, must lie above the equilibrium locus in the *H-N* diagram.

Equation (4) can be solved numerically using a shooting method. This consists of a search for the appropriate coefficient C_λ as defined by the asymptotic behavior (i.e., for $r \geqslant r_0$, where r_0 is so large that the nonlinear term is negligible) of the solutions of Eq. (4) for a given λ,

$$\phi_\lambda(r) \approx C_\lambda \exp(-\lambda^{1/2} r) \Big/ (\lambda^{1/2} r)^{1/2} \quad \text{for} \quad r \geqslant r_0, \tag{8}$$

which, after a numerical integration of Eq. (4) from $r = r_0$ to $r = 0$, yields

$$d\phi_\lambda(r)/dr|_{r=0} = 0. \tag{9}$$

For a given λ, because of the nonlinearity for $r < r_0$, only discrete values of C_λ can fulfill the boundary condition (9) and the smallest C_λ defines the ground-state solution (at least, from our experience, in the cases we have considered). Figure 2 shows some features of the ground-state solutions in the 2D case for the nonlinearity (3) as a function of λ, namely, the maximum amplitude $\phi_\lambda(0)$ and the root-mean-square (rms) radius ρ_λ. It is seen that as $\lambda \to 0$, $\phi_\lambda(0)$ vanishes but ρ_λ goes to infinity, while as $\lambda \to 1$, both $\phi_\lambda(0)$ and ρ_λ go to infinity, a result familiar from previous approximated calculations [1,25,27]. As a result, the power N remains finite for $\lambda \to 0$, i.e., $N = N_c$, while $N \to \infty$ for $\lambda \to 1$.

III. OSCILLATIONS NEAR EQUILIBRIUM

We will be interested in the behavior of the radial solutions $u(r,t)$ of Eq. (2) when the initial condition $u(r,0)$ differs somewhat from some equilibrium solution $\phi_\lambda(r)$ of Eq. (4) as

$$u(r,0) = (1-\varepsilon)\phi_\lambda((1-\varepsilon)r), \tag{10}$$

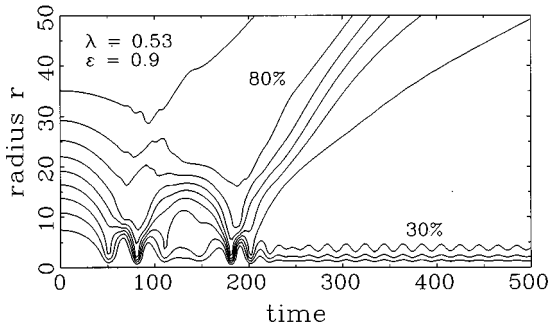

FIG. 3. Normalized included power contours in the radius vs time plane for an initial state rather far from equilibrium. In this example $\varepsilon = 0.9$ and $\lambda = 0.53$.

where the deviation parameter ε is such that $0 < \varepsilon < 1$. This definition allows us to control the deviations from the equilirium solutions by means of the parameter ε and also ensures that $N = N_\lambda$ for all times (since N is an integral of motion). Returning to Fig. 1 again, the representative point of $u(r,0)$ in the *H-N* diagram is then displaced horizontally to the right with respect to the representative point of $\phi_\lambda(r)$ on the equilibrium locus. Therefore, one begins further away from *any* equilibrium solution as ε increases. We have checked that the following results would remain essentially unchanged if a less simple choice for the initial condition would have been made [for example, a Gaussian function with the same power N and the same maximum amplitude *or* the same mean radius as $\phi_\lambda(r)$].

For rather large deviation of the initial state from equilibrium, i.e., $\varepsilon \approx 1$, the beam generally undergoes complicated oscillations [22] and a significant fraction of N escapes from the central beam (i.e., radiation) [21]. A nice example, where $\varepsilon = 0.9$ and $\lambda = 0.53$, is illustrated in Fig. 3, which shows the level contours of the normalized included power [4],

$$\nu(r,t) = N_\lambda^{-1} \int_0^r |u(r,t)|^2 r \, dr,$$

which is such that $0 \leqslant \nu(r,t) < 1$. It is seen that in the time interval $0 < t < 250$, the beam oscillates in a rather violent and complicated way and that about 70% of the initial power N_λ is radiated away, leaving only about 30% unradiated. For $t > 250$ the self-focused beam reaches a gently oscillating state that is not far from the equilibrium solution characterized by $\lambda \approx 0.31$ (a value smaller than the initial one). It should be noticed that, in general, the rate of radiation emission is much smaller than in the example of Fig. 3 for $t < 250$ and, due to the natural limitations of the numerical calculations, it is hard to observe an asymptotic state so close to equilibrium as the one seen in Fig. 3 for $t > 250$. However, since in these cases radiation seems to be continually emitted as a function of time, it is plausible that an asymptotic *nearly* equilibrium state, similar to the one of Fig. 3 for $t > 250$, is always reached (as long as $N > N_c$ and $H < 0$).

There is a close relationship between the radiation emission and the beam's evolution towards equilibrium, as discussed in Ref. [23], which treatment we will recapitulate for convenience with some further elaboration. Consider $n(r,t)$ and $h(r,t)$, which are defined in a way similar to

N and H [Eqs. (5) and (6)] respectively, but with the difference that the integration is not performed over the whole transverse plane but over a finite transverse surface S of radius r instead. While N and H are time independent, $n(r,t)$ and $h(r,t)$ in general are not because of transfers through the boundary of S. Assume that we choose S large enough so that practically $n(r,t)=N$ and $h(r,t)=H$ at $t=0$, H and N corresponding to a particular initial condition $u(r,0)$. Because of the radiation emission from S and because the nonlinearity is negligible outside S, the contributions to N and H outside S [i.e., $N-n(r,t)$ and $H-h(r,t)$] are positive and increase in time. Thus the representative point $(n(r,t),h(r,t))$ in the H-N diagram starts at the point (H,N) and evolves inside the (curved) triangle formed by the equilibrium locus and the two perpendicular lines $N=N$ and $H=H$ (see Fig. 1). As the representative point approaches the equilibrium locus [necessarily near an equilibrium state characterized by a λ smaller from the one appearing in Eq. (10)] the oscillation amplitude is then expected to decrease, to become more regular, with radiation emitted at a decreasing rate, as illustrated in Fig. 3. (An interesting consequence is that the upper bound on the amount of radiation emitted is given by $N-N_F$, where N_F is the value of N corresponding to the intersection of the equilibrium locus and the vertical line $H=H$.) Therefore, the radiation emission can be seen as the means used by the nonlinear system to reach a state closer to equilirium.

Let us now consider initial states very close to equilibrium, i.e., $\varepsilon \ll 1$, which, as discussed above, corresponds to investigating the beam's behavior for large times (or to the beamlet's behavior in the filamentation process for large times [21]). A systematic investigation of the time behavior of the solutions of Eq. (2), as a function of λ, reveals that there are three main types of behavior or oscillations, which we will denote A, B, and C and which occur in rather well-defined ranges of λ. These appear after a transient that lasts for only a few oscillation periods and can be characterized by the oscillations of the field amplitude $|u(0,t)|$. (In fact, the choice of any radius r, other than $r=0$, located in a region where the nonlinearity is non-negligible, i.e., for $r<r_b$, where $r_b \approx 2\rho_\lambda$, would lead to the same conclusions; the choice $r=0$ is only a matter of convenience.) Figure 4 shows the quantity $I_0'(t)= dI_0(t)/dt$, where $I_0(t)=|u(0,t)/\phi_\lambda(0)|^2$ for the three types of oscillations. [The time derivative of $I_0(t)$ was taken in order to remove the constant part of the intensity and thus simplify the analysis.] Type-A behavior occurs for $0<\lambda<0.47$ (approximately) and is characterized by a damped oscillation having a rather well-defined single (real) frequency since the zeros of $I_0'(t)$ are regularly spaced and thus correspond to a well-defined period after the short transient. Type-B behavior is the simplest one: It happens approximately for $0.47<\lambda<0.84$ and is characterized by an undamped, or at most very weakly damped, oscillation having a well-defined single frequency, as can be seen in Fig. 5(a) which shows $|\tilde{I}_0'(\omega)|$, where $\tilde{I}_0'(\omega)$ is the discrete Fourier transform of $I_0'(t)$. Finally, type-C behavior is seen for λ values greater than for type-B behavior (i.e., approximately for $0.84<\lambda<1$) and corresponds, like type-B behavior, to an undamped (or at most very weakly damped) oscillation, but now with two or more well-defined frequencies that generally do not seem to be in simple ratios, as can be seen in Fig. 6, which shows the power spectrum for three different values of λ for $\lambda>0.84$. As λ increases, new small-frequency spikes appear at critical values λ_n near frequencies $\omega=\lambda_n$ and then move towards smaller ω while increasing in amplitude as λ is further increased.

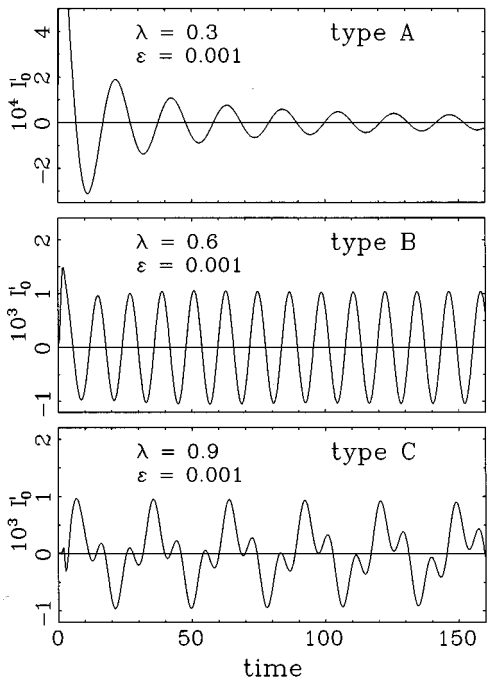

FIG. 4. Examples of the three observed main types of oscillations (types A, B, and C) near equilibrium.

These observations hold only for small perturbation amplitudes ($\varepsilon \ll 1$). As ε increases gradually, secondary sharp spikes corresponding to multiples of the primary frequencies (i.e., those that are seen when $\varepsilon \ll 1$) appear in the power

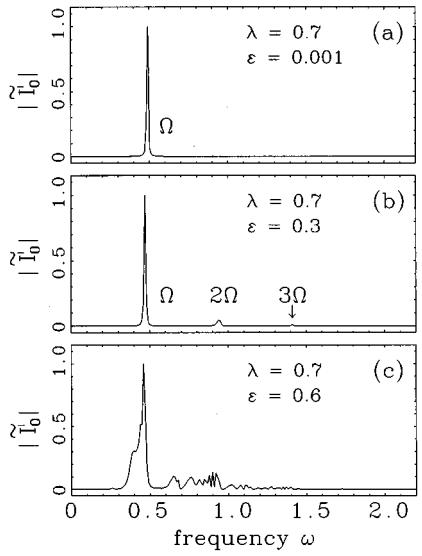

FIG. 5. Fourier spectrum of $I_0'(t)$ (see the text for the definition) for initial beams near the equilibrium solution $\lambda=0.7$, for the initial displacements $\varepsilon=0.001$ (a), 0.3 (b), and 0.6 (c).

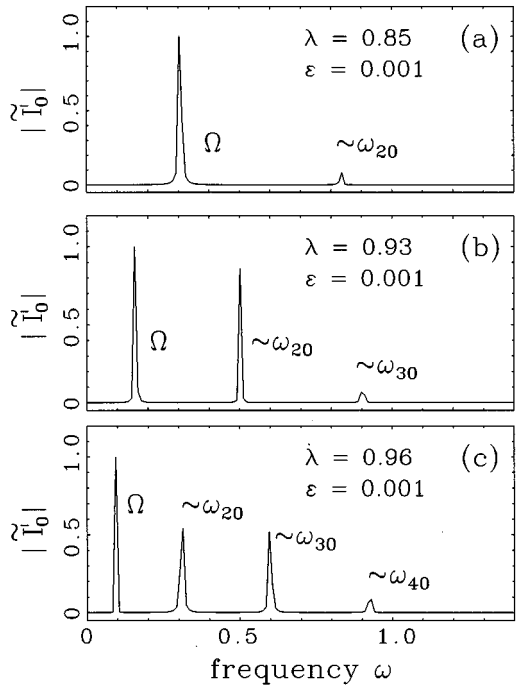

FIG. 6. Fourier spectrum of $I_0'(t)$ (see the text for the definition) for initial beams near the equilibrium solutions characterized by $\lambda=0.85$ (a), 0.93 (b), and 0.96 (c), for the initial displacement $\varepsilon=0.001$. The values of λ correspond approximately to the appearance of a new frequency spike on the right of the spectrum.

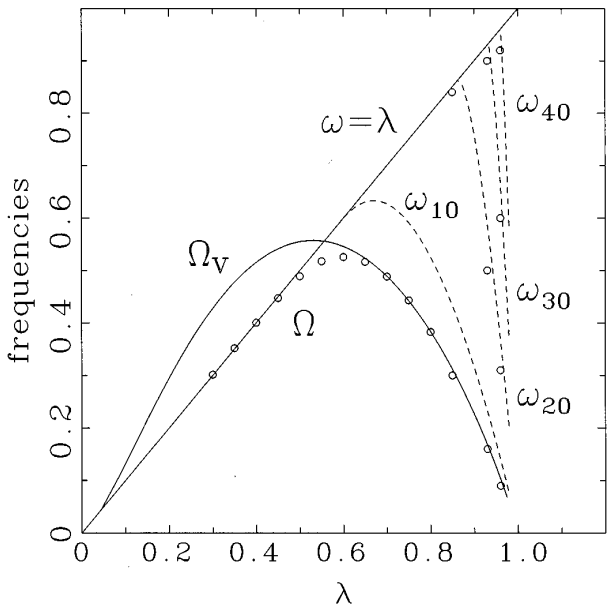

FIG. 7. Frequencies as a function of λ. Small circles correspond to observed frequencies (for $\lambda>0.84$ several frequencies coexist for the same value of λ). The set of smallest observed frequencies is labeled Ω. Dashed curves correspond to the frequencies $\omega_{n0}=E_n-E_0$ for $n=1$–4. The curve labeled Ω_V is obtained from a variational calculation.

spectrum. For type-*A* and -*B* behavior, the secondary spikes correspond to multiples of the primary frequency. For some critical value of ε, which depends on λ, the power spectrum becomes filled with a background noise. This is illustrated in Fig. 5 for $\lambda=0.7$ (corresponding to a type-*B* behavior) for various ε. As can be seen in this figure, for $\varepsilon=0.001$ a single spike is present in the power spectrum at the frequency $\omega=\Omega\approx0.48$ [Fig. 5(a)]. When $\varepsilon=0.3$, secondary spikes can be seen at the frequency 2Ω and 3Ω [Fig. 5(b)] (other spikes at 4Ω , 5Ω, . . . are also present, but are much weaker). When $\varepsilon=0.6$, the main spike can still be distinguished, but a continuum of new structures appear at high frequencies in the power spectrum [Fig. 5(c)]. For type-*C* behavior, as ε increases gradually, secondary spikes corresponding to multiples of the basic frequencies appear in the power spectrum as for type-*A* and -*B* behavior, but, in addition, spikes located at the beat frequency combinations $|\omega_i\pm\omega_j|$, where $i,j(i\neq j)=1,2,\ldots$, also appear (among others more difficult to identify). As for types *A* and *B*, the power spectrum becomes filled with a background noise when ε is further increased.

For the simplest type, *B*, numerical investigations reveal that the beam amplitude evolves nearly as the *N*-conserving, self-similar form

$$|u(r,t)|\approx(1+\gamma(t))\,\phi_\lambda([1+\gamma(t)]r), \tag{11}$$

where $\gamma(t)$ is a periodic function. To first order in $\gamma(t)$, Eq. (11) is

$$|u(r,t)|\approx\phi_\lambda(r)+\sigma_1(r)\,\gamma(t) \quad \text{for} \quad |\gamma(t)|\ll1, \tag{12}$$

where the function $\sigma_1(r)=\phi_\lambda(r)+\partial\phi_\lambda(r)/\partial r$ is easily shown to be orthogonal to $\phi_\lambda(r)$ and to have a single node at some distance r. Owing to the fact, mentioned above, that the observed frequencies are r independent (as long as $r<r_b$), Eq. (12) generalizes as follows, when several well-defined frequencies are present for a given λ (as for type-*C* oscillations):

$$|u(r,t)|\approx\phi_\lambda(r)+\sum_{n=1}\sigma_n(r)\,\gamma_n(t) \quad \text{for} \quad |\gamma_n(t)|\ll1, \tag{13}$$

where the sum is over all frequencies. When damping of the oscillations occurs (i.e., for type *A* oscillations for any value of ε and for all types when ε is not very small) the $\gamma_n(t)$ in Eq. (13) are then slowly decreasing functions of time. Notice that the radiation component, associated with the damping of the oscillations, is not included in Eq. (13), which is then expected to hold only in the region where the nonlinearity is non-negligible, i.e., for $r<r_b$.

The oscillation frequency values as a function of λ, for $\varepsilon\ll1$, are shown in Fig. 7. Small circles correspond to the frequencies obtained from the direct numerical solutions of Eq. (2). Note that for $\lambda>0.84$ there is more than one frequency for a given value of λ (type-*C* behavior). The lowest oscillation frequency ω, which is unique for $\lambda<0.84$, forms a smooth curve for $\lambda>0.84$, which becomes the smallest of the multiple frequencies. We will refer to this frequency as $\Omega(\lambda)$. It can be seen that for $\lambda<0.47$ (type-*A* behavior), $\Omega\approx\lambda$, and that for $\lambda\approx0.6$, Ω has a maximum and goes to 0 as λ approaches 1.

The quasi-self-similar behavior of the small radial oscillations (at least for type *B*) reported above [see Eq. (11)]

naturally suggested using this property to do approximate calculations [25,27,28]. Anderson and Bonnedal [27] performed a variational calculation for the nonlinearity of interest here [Eq. (3)], starting from the simple trial function

$$u(r,t)\approx A(t)\exp[-r^2/2R(t)^2+ib(t)r^2]. \tag{14}$$

Of course, $A(t)$ and $R(t)$ are not independent since $A(t)^2R(t)^2=2N$, and N [see Eq. (5)] is time independent. The approximate equilibrium solution can be written as

$$\phi_\lambda(r)\approx A_\lambda\exp(-r^2/2R_\lambda^2), \tag{15}$$

where the equilibrium radius R_λ is related to the equilibrium amplitude A_λ as [27]

$$R_\lambda=A_\lambda(-\mathrm{dilog}(1+A_\lambda^2)-\ln(1+A_\lambda^2)+A_\lambda^2)^{-1/2}, \tag{16}$$

in which $\mathrm{dilog}(x)\equiv\int_1^x\ln(t)(t-1)^{-1}dt$ is the usual dilogarithm function [29]. For small oscillations near equilibrium, the oscillation frequency is [27]

$$\Omega_V=2\sqrt{\frac{2}{R_\lambda A_\lambda}}\left(-2\,\mathrm{dilog}(1+A_\lambda^2)-3\ln(1+A_\lambda^2)+\frac{A_\lambda^2}{1+A_\lambda^2}\right)^{1/2}. \tag{17}$$

From Eq. (4) one can express λ in terms of A_λ and $R_\lambda(A_\lambda)$, using Eq. (15),

$$\lambda=R_\lambda^{-2}+A_\lambda^{-2}\ln(1+A_\lambda^2)-1, \tag{18}$$

and thus plot $\Omega_V(A_\lambda)$ against $\lambda(A_\lambda)$ as in Fig. 7. It is worth noticing that for the same trial function, Eq. (14), we found that the virial method [12] also yields Eqs. (15)–(17), although an assumption about the phase in the trial function is not required for this method.

From Fig. 7 it is clear that $\Omega_V(\lambda)$ constitutes an excellent approximation of $\Omega(\lambda)$ for $\lambda>0.65$ (for which Ω_V is less than λ), while the agreement is poorer for lower λ values. The poor agreement for $\lambda<0.65$ is not really surprising in view of the fact that the trial function (14) is not able to take into account the oscillation damping or the radiation component that characterizes type-*A* behavior. This is a warning that Ω_V is unlikely to exist with a real part only, as originally assumed. While the ''overtone frequencies,''i.e., those above Ω, appearing for $\lambda>0.84$, can, in principle, also be obtained from the appropriate trial functions by means of the virial or the variational method, we will not perform these calculations here since, as we will see in the next section, these frequencies can be interpreted in a very simple way from a quantum-mechanical point of view.

IV. ANALYSIS

A. General discussion

In this section we will show that the oscillations near equilibrium examined in the preceding section share many features with some well-known quantum-mechanical effects. In particular the multiple frequencies observed in type-*C* oscillations for $\varepsilon\ll 1$ will be shown to correspond to Rabi-like oscillations between energy levels [30], while the radiation emission, which is responsible from the damping of the oscillations observed, for instance, in type-*A* oscillations, appears to be an effect analogous to photoionization [31].

Let us first rewrite Eq. (2) in a form familiar in quantum mechanics

$$i\frac{\partial u}{\partial t}-(H_0+\delta V)u=0, \tag{19}$$

where $H_0=-\nabla_\perp^2+V_0$ is the unperturbed Hamiltonian, with

$$V_0(r)=-f(|u_\lambda(r,t)|^2), \tag{20}$$

as the unperturbed potential, which will be assumed to be known [after solving Eq. (4) for the equilibrium solution $u_\lambda(r,t)$], and a perturbing potential

$$\delta V(r,t)=-f(|u(r,t)|^2)-V_0(r). \tag{21}$$

For the given unperturbed potential V_0, stationary solutions of Eq. (19), i.e., when $\delta V=0$, are of the form $u(r,t)\propto u_E(r,t)\equiv\xi_E(r)\exp(-iEt)$, where $\xi_E(r)$ are the normalized eigenfunctions satisfying the *linear* Schrödinger equation

$$(H_0-E)\xi_E=0. \tag{22}$$

Here E is equivalent to energy in quantum mechanics. Comparing Eqs. (22) and (4), one can see that the ground-state energy level of the eigenvalue equation (22) is $E=E_0\equiv-\lambda$ and that the corresponding eigenfunction is $\xi_{E_0}(r)=N_\lambda^{-1/2}\phi_\lambda(r)$, so that $u_E(r,t)=N_\lambda^{-1/2}u_\lambda(r,t)$. Of course, Eq. (22) may have other discrete states (excited states) corresponding to the energies $E_1\leqslant E_2\leqslant E_3\leqslant\cdots<0$ and has certainly a continuum of states (i.e., unbound states) for $E\geqslant 0$. Since H is an Hermitian operator, the eigenfunctions ξ_E of Eq. (22) can be defined so that they form a complete basis of *orthonormal* functions on which, in particular, the solutions of Eq. (19) can be expanded.

For the perturbing potential $\delta V(r,t)$, we have to first order in $|u|-\phi_\lambda$,

$$\delta V\approx-\left(|u|-\phi_\lambda\right)\left.\frac{df(q^2)}{dq}\right|_{q=\phi_\lambda}. \tag{23}$$

From the observations about small oscillations near equilibrium reported in Sec. III, one obtains an approximate general form for $\delta V(r,t)$: substituting Eq. (13) in Eq. (23) yields

$$\delta V(r,t)\approx\sum_n\delta\widetilde{V}_n(r)\exp(-\eta_n t)\cos(\omega_n t+\alpha_n)\quad\text{for}\quad r<r_b, \tag{24}$$

where the sum is performed over all frequencies ω_n present for a given λ. Here $\delta\widetilde{V}_n(r)$ are time-independent functions, α_n are constant phases, and η_n are small positive constants that we introduce to approximate the damping of the oscillations due to radiation loss. The condition $r<r_b$ has been added in Eq. (24) because the latter may not hold outside this range, where radiation may take place. In fact, only the range $r<r_b$ will be useful in the following discussion.

1. Rabi oscillations

We now consider type-C oscillations, i.e., multiple undamped frequencies. Viewing Eq. (19) from a quantum-mechanical point of view leads one naturally to suspect that there is some relationship between the frequencies observed in type-C oscillations and the transition frequencies $\omega_{nm}=E_n-E_m$, where the E_i are the eigenvalues of Eq. (22). These expectations prove to be fulfilled, as can be seen in Fig. 7, where the frequencies ω_{n0} for $n=1-4$ are shown as dashed lines. [The first four excited energy levels E_1–E_4 were calculated numerically by solving Eq. (22) for various unperturbed potentials characterized by the parameter $\lambda=-E_0$]. While the overtone frequencies observed in type-C oscillations are seen to be close to ω_{20}, ω_{30}, and ω_{40}, the agreement between Ω (or Ω_V) and ω_{10} is not nearly so good. In this connection, it is worth noticing that, in linear two-level systems in which the perturbation is stationary, the actual transition frequency approaches the difference between the two energy levels, say E_n and E_m, when this value is large with respect to the matrix elements $\langle \xi_{En}|\delta V|\xi_{Em}\rangle \equiv \int \xi_{En}^{*}\delta V\ \xi_{Em}dx\ dy$ [30]. This feature appears in Fig. 7, since the agreement between the observed frequencies and ω_{n0} seems to improve as n increases. This analogy with a linear stationary two-level system leads us to the following two provisional conclusions. The first is that the excited states ($n\geqslant 1$) are relatively strongly coupled with the state $n=0$ and only weakly between themselves since the related frequencies ω_{nm}, where $n>m\geqslant 1$, are not seen in the power spectrum. The second conclusion is that the dominant term in the perturbing potential δV, Eq. (24), has a frequency significantly smaller than ω_{n0} for $n\geqslant 2$ since it seems to act as a nearly constant (or zero-frequency) perturbation. It is thus plausible that the term in the perturbing potential δV corresponding to the frequency Ω is indeed responsible from the excitation of the Rabi-like oscillations between the energy levels of the perturbed system.

2. Radiation emission

Let us now investigate the possible transitions to the continuum that the perturbing potential Eq. (24) may cause. The basic idea is in the association of the radiation emission, inferred in Sec. III, for instance, for type-A oscillations, with the well-known photoionization effect in quantum mechanics, in which the probability to find a bound electron in its initial stationary state irreversibly decreases in time when the frequency of an external perturbation (for instance, an electromagnetic field) is such that $\omega\geqslant -2\pi E_b/h$, where E_b is the binding energy of the electron and h is the Planck constant, a condition that ensures that the induced state of the electron is in the continuum. One deals with such a problem by means of the standard time-dependent perturbation theory in which one calculates a transition probability $dP_E=N_\lambda^{-1}|\langle u_E|u\rangle|^2 dE$ from the initial well-defined initial state u_λ to the state of the continuum u_E ($E\geqslant 0$) between the energy E and $E+dE$ [31].

In our case, we have that $u(r,t)\rightarrow u_\lambda(r,t)$ as $t\rightarrow\infty$, i.e., the beam tends to equilibrium asymptotically (escaping radiation can be neglected as $t\rightarrow\infty$, as a first approximation). This statement is not really in contradiction with the observations about type-B and -C oscillations made in Sec. III since nothing is said about the characteristic time of convergence to equilibrium. Given the perturbation of the form Eq. (24), one can repeat the standard derivation of the transition probability rate dw_E found in textbooks, with the important difference that here the perturbation is ''switched on'' in the far future (instead of $t=0$), since the equilibrium state appears for $t\rightarrow\infty$, and one then has to calculate the transition probability for finite values of t. One finds the familiar ''one-photon transition'' probability rate

$$dw_E\approx\frac{\pi}{2N_\lambda}\sum_n |\langle u_E|\delta\tilde{V}_n|u_\lambda\rangle|^2\frac{\eta_n/\pi}{(E+\lambda-\omega_n)^2+\eta_n^2}\ dE. \tag{25}$$

Notice that the $\delta\tilde{V}_n$, and therefore δV, need only be known for $r<r_b$ ($r_b\approx 2\rho_\lambda$) since the integrand of the nth integral vanishes outside this range because of u_λ. When η_n goes to zero, the nth ratio in the summation is replaced by $\delta(E+\lambda-\omega_n)$, where $\delta(x)$ is the Dirac delta function. As in quantum mechanics, Eq. (25) indicates that irreversible losses to the continuum states ($E\geqslant 0$), i.e., radiation, occur *only* when $\omega_n\geqslant\lambda$ for at least one ω_n (assuming the η_n small) since only in this case the transition probability to the continuum is appreciable.

Now, referring to Fig. 7, one can see that for $\lambda>0.47$ (types B and C) one has $\omega_n<\lambda$ for all n (except possibly at unimportant isolated points in the case of type-C oscillations) and therefore, according to Eq. (25), no radiation should be produced, in agreement with the observations made in Sec. III. For $\lambda<0.47$ (type-A oscillations), the unique oscillation frequency observed is such that $\omega\approx\lambda$, which indicates, according to Eq. (25), that transitions to the continuum states close to $E=0$ do occur. Once again this conclusion is in agreement with the observations reported in Sec. III, where the emission of radiation in the case of type-A oscillations was inferred from the damping of the oscillations. A link is thus established between the value of the oscillation frequency and the emission (or not) of radiation. The perhaps intriguing fact that the transitions to the continuum states, for type-A oscillations, are apparently so close to $E=0$ will be clarified at the end of this section by considering, as a particular case analogous to the present discussion, the 1D CNLSE, for which analytical solutions are known, which presents the same features as the type-A oscillations described in Sec. III.

We now consider the cases where the initial states are not so close to equilibrium. When ε increases gradually, we noticed that secondary frequencies and eventually background noise appear in the power spectrum [Fig. 5]. While, for example, for type-B oscillations, the frequency Ω is too small to ensure a transition to states in the continuum, the secondary frequencies 2Ω, 3Ω, . . . , or the frequencies forming the background noise, as ε is further increased, are greater than λ, i.e., large enough to allow such transitions. According to Eq. (25), one expects, therefore, radiation to be produced, and consequently oscillations to be damped, until ε decreases sufficiently as the beam gets close to equilibrium, i.e., so that the secondary frequencies come to play a negligible role. Thus, for type-B and -C oscillations the damping of the oscillations should eventually stop, while the damping continues for type-A oscillations since in this case the radia-

tion emission is not due to the secondary frequencies but to the primary one, Ω. This description of the evolution of the self-focused beam starting not so close from equilibrium, made on the basis of Eq. (25), is in agreement with the numerical solutions, where a damping of the oscillations is always observed initially when ε is not very small (see Fig. 3, for instance). Of course, in principle, the secondary frequencies exist even when ε is arbitrarily small, although their corresponding amplitude in the power spectrum is very small. Consequently, type-*B* and -*C* behavior should lead asymptotically, *but over a much longer time scale*, to an equilibrium state as for type-*A* oscillations. Besides this, the analog of ''multiphoton transitions,'' which correspond to higher-order terms in Eq. (25), may also contribute to the transitions to the continuum. In sum, the main difference between type-*A* oscillations, on the one hand, and types *B* and *C*, on the other hand, is that for type *A* the primary frequency Ω ensures the transitions to the continuum, while for types *B* and *C* they are enabled only by the secondary frequencies, whose influence decreases rapidly as ε decreases, and probably by multiphoton-transition-like processes, both of which are effects of higher order.

B. One-dimensional cubic nonlinearity

Let us now compare the above general analysis with analytical solutions for the 1D CNLSE case, which includes the complete behavior. The equilibrium ground-state solutions of Eq. (4) are

$$u_\lambda(x,t)=\sqrt{2\lambda}\,\mathrm{sech}(\sqrt{\lambda}x)\exp(i\lambda t). \tag{26}$$

Setting $u=u_\lambda+\delta u$ and using the fact that $u_\lambda(x,t)$ satisfies Eq. (22), particular solutions of Eq. (19) linearized about these equilibrium solutions have been obtained by Gordon [33] and are, in our notation,

$$\delta u(x,t)=-2\frac{\partial^2 g}{\partial x^2}+4\sqrt{\lambda}\tanh(\sqrt{\lambda}x)\frac{\partial g}{\partial x}-2\lambda g\tanh^2(\sqrt{\lambda}x)$$
$$+2\lambda g^*\mathrm{sech}^2(\sqrt{\lambda}x)\exp(2i\lambda t), \tag{27}$$

where $g(x,t)$ is any solution of the free Schrödinger equation

$$i\frac{\partial g}{\partial t}+\frac{\partial^2 g}{\partial x^2}=0. \tag{28}$$

One can see that for large times $\delta u(x,t)$ is not localized within the range of the equilibrium solutions (26) (i.e., $|x|<x_b\approx 2\lambda^{-1/2}$) because $g(x,t)$ is spread out (diffracted) as time increases. This ensures that $u(x,t)\to u_\lambda(x,t)$ (for $|x|<x_b$) as $t\to\infty$, as required. Also, it is easy to see that, to first order in g (or its derivatives), i.e., for small oscillations, $|u(x,t)|$ oscillates with the frequency $\omega=\lambda$ about $|u_\lambda(x,t)|$, with an amplitude variation proportional to g (or its derivatives), which necessarily decreases in time since $g(x,t)$ does within the range of the equilibrium solution. Therefore, the small oscillations of the 1D CNLSE present the same features as the type-*A* damped oscillations observed in Sec. III [i.e., in the 2D case with the saturable nonlinearity (3)] with the difference that here it occurs for all possible values of λ, which now ranges from 0 to ∞ since the nonlinearity $f(s)=s$ does not saturate. (It is interesting to note that Anderson's variational model [28] for the 1D CNSLE, which does not take into account the radiative field, yields the oscillation frequency $\omega=\lambda\pi/3$, which is somewhat greater than the correct frequency λ, in the same way as the variational estimate Ω_V [Eq. (17)] was greater than the observed frequency Ω for type-*A* oscillations.)

The unperturbed potential $-f(|u_\lambda|^2)=-|u_\lambda|^2=-2\lambda\ \mathrm{sech}^2(\sqrt{\lambda}x)$ is such that its depth increases as λ, but its width decreases as $\lambda^{-1/2}$. For 1D square well potentials, the product depth$\times$width^2 determines the number of bound states [32]. The fact that this quantity is nearly constant here explains why the type-*C* behavior (multiple oscillation frequencies) is not observed for the 1D CNLSE: The unperturbed potentials have no excited states. As shown in Fig. 2, the depth and width of the 2D unpertured potential corresponding to the saturable nonlinearity (3) both increase as λ increases, which allows excited states. Numerical investigations show that this is not due to the number of transverse dimensions but rather to the form of the nonlinearity. As a matter of fact, in one dimension the saturable nonlinearity (3) presents the same three types of behavior as in two dimensions. Only small quantitative differences distinguish the two cases: For instance, in the 1D case, type-*A* behavior happens for $0<\lambda<0.47$, type *C* for $0.89<\lambda<1$, and type *B* in between.

According to Eq. (25), radiation should be emitted in the case considered here since the unique oscillation frequency is such that $\omega=\lambda$, which implies transitions to the continuum states of energies around $E=0$ after the transient. One can see that the radiation field given by Eq. (27) is fully consistent with this finding. As a matter of fact, solutions of Eq. (28) can be written as

$$g(x,t)=\int_{-\infty}^{+\infty}\tilde{g}(k)\exp[i(kx-k^2t/2)]dk. \tag{29}$$

Here k is related to E, appearing in Eq. (22), as $k^2=E$. Now, assume that the initial state $u(x,0)$ is real and even. [The assumption that $u(x,0)$ is even is similar to the radial symmetry assumption in two dimensions.] Consequently, from Eq. (27), $g(x,0)$ is also real and even and thus $\tilde{g}(k)$ is real. Outside the equilibrium solution, Eq. (27) is

$$\delta u\approx -2\frac{\partial^2 g}{\partial x^2}+4\sqrt{\lambda}\frac{x}{|x|}\frac{\partial g}{\partial x}-2\lambda g,\quad \text{for}\quad |x|>r_b. \tag{30}$$

Substituting Eq. (29) in Eq. (30) and using the fact that the leading contributions of the integrand occur when its phase is stationary, i.e., when $k\approx x/t$, one concludes that the Fourier modes around $k=0$, or $E=0$, are indeed the dominant modes in $g(x,t)$, and therefore in $\delta u(x,t)$, when t is large, as asserted above.

V. SUMMARY AND CONCLUSIONS

We have investigated the behavior of radially symmetric solutions of the 2D NLSE for the generic saturable nonlinearity (3), near the equilibrium solutions $u_\lambda(r,t)$, which are characterized by a single parameter λ ranging between 0 and

1 in our case. When the initial beam is rather far from any equilibrium solution and when the integral of motion are such that $N \geqslant N_c$ and $H<0$, the beam initially approaches some equilibrium solution in a manner characterized by irregular oscillations accompanied by a significant amount of radiation emission. As the beam gets closer to equilibrium, its behavior simplifies considerably and this asymptotic phase of its evolution constituted the main subject of our investigations. Contrarily to the well-known 1D CNLSE, where only damped single-frequency oscillations (type *A*) are observed, one can see, in addition, in the case we studied, single (type-*B*) and multiple (type-*C*) frequencies of practically undamped oscillations. We also observed that when the oscillations are not so close to equilibrium, secondary frequencies appear in the Fourier spectrum, which are multiples of the primary ones and also simple combinations of them. For oscillations rather far from equilibrium the secondary frequencies combine and proliferate to form a noisy spectrum.

We considered our problem from a quantum-mechanical formulation. Very general features of the perturbation (mostly the characteristic frequencies) were taken from the numerical solutions. We found that the observed multiple frequencies of the oscillations (type *C*) corresponded approximately to the transition frequencies from ground to excited states ω_{n0} of the unperturbed potential, the agreement improving as ω_{n0} increases, in a way that is familiar in simple two-level systems in quantum mechanics. Our analysis has also revealed a link between the oscillation frequencies and the emission of radiation: when at least one frequency ω_n characterizing the perturbation is such that $\omega_n \geqslant \lambda$ ($-\lambda$ being equal to the energy of the fundamental bound state) the latter is then able to induce a transition from the fundamental state (equilibrium, bound solution) to the continuum (unbound states of positive energy, i.e., radiation) in a way similar to the well-known photoionization effect. Such a frequency can be found for type-*A* oscillations, but not for type-*B* and -*C* oscillations, a fact that is consistent with our observations of the numerical solutions. The exactly solvable 1D CNSLE (for which only type-*A* oscillations are observed) has been found to be in agreement with this general analysis. The main difference between linear quantum mechanics and the nonlinear system considered here is that here the perturbation is not imposed from outside: The system generates it by its own means.

For powers large with respect to critical ($N/N_c \gg 1$), the beam is likely to break up into several beamlets if the initial beam is not perfectly symmetric radially and rather far from the equilibrium locus in the *H*-*N* diagram (see Fig. 1). We have shown elsewhere that when filamentation occurs, the beamlets approach asymptotically equilibrium solutions, ranging typically from $N/N_c=1$ to 20 [21]. For the nonlinearity considered in that work, this range includes only type-*A* and -*B* oscillations, since type-*C* oscillations only occur for $N/N_c > 75$ or $\lambda > 0.87$ [while for the nonlinearity (3) type-*C* oscillations occur for $N/N_c > 172$]. Therefore, type-*C* oscillations would seem to be unlikely to be observed in practical situations. If two independent degrees of oscillation freeedom were allowed, rather than the single radial one imposed in the present study, one would likely observe a richer and more complex variety of behavior near equilibrium than that reported in the present paper, such as transverse quadrupole oscillations, for instance. It is plausible, however, as asserted in Ref. [24], that the anisotropic modes would damp out and that the purely radial oscillations would come to dominate. In that case the results of the present study would hold asymptotically in this more general context. This interesting topic is beyond the scope of the present work and will constitute the subject of a future investigation.

ACKNOWLEDGMENTS

This work was supported by the Ministère de l'Éducation du Québec and by the Natural Sciences and Engineering Research Council of Canada under Strategic Grant No. STR 0149641.

[1] C. E. Max, Phys. Fluids **19**, 74 (1976).
[2] A. J. Schmitt, Phys. Fluids **31**, 3079 (1988).
[3] P. Kaw, G. Schmidt, and T. Wilcox, Phys. Fluids **16**, 1522 (1973).
[4] B. I. Cohen B. F. Lasinski, A. B. Langdon, and J. C. Cummings, Phys. Fluids B **3**, 766 (1991).
[5] H. A. Rose and D. F. Dubois, Phys. Fluids B **5**, 3337 (1993).
[6] V. Tikhonenko, J. Christou, and B. Luther-Davies, Phys. Rev. Lett. **76**, 2698 (1996); J. Opt. Soc. Am. B **12**, 2046 (1995).
[7] B. Luther-Davies, R. Powles, and V. Tikhonenko, Opt. Lett. **19**, 1816 (1994).
[8] J. W. Grantham, H. M. Gibbs, G. Khitrova, J. F. Valley, and Xu Jianjin, Phys. Rev. Lett. **66**, 1422 (1991).
[9] Guo-Zheng Sun, E. Ott, Y. C. Lee and P. Guzdar, Phys. Fluids **30**, 526 (1987).
[10] A. B. Borisov, O. B. Shiryaev, A. McPherson, K. Boyer, and C. K. Rhodes, Plasma Phys. Control. Fusion **37**, 569 (1995).
[11] K. Konno and H. Suzuki, Phys. Scr. **20**, 382 (1979).
[12] For a review see J. J. Rassmussen and K. Rypdal, Phys. Scr. **33**, 481 (1986), and references therein.
[13] A. Hasegawa, *Optical Solitons in Fibers*, 2nd ed. (Springer-Verlag, Berlin, 1989), p. 18.
[14] V. E. Zakharov and A. B. Shabat, Zh. Éksp. Teor. Fiz. **61**, 118 (1971) [Sov. Phys. JETP **34**, 62 (1972)].
[15] P. Kelley, Phys. Rev. Lett. **15**, 1005 (1965).
[16] M. D. Feit and J. A. Fleck, J. Opt. Soc. Am. B **5**, 633 (1988).
[17] P. B. Corkum, C. Rolland, and T. Srinivasan-Rao, Phys. Rev. Lett. **57**, 2268 (1986); P. B. Corkum and C. Rolland, in *Self-Focusing and Continuum Generation in Gases*, edited by R. R. Alfano (Springer-Verlag, New York, 1989).
[18] S. N. Vlasov, L. V. Piskunova, and V. I. Talanov, Zh. Éksp. Teor. Fiz. **75**, 1602 (1978) [Sov. Phys. JETP **48**, 808 (1978)].
[19] J. M. Soto-Crespo, D. R. Heatly, E. M. Wright, and N. N. Akhmediev, Phys. Rev. A **44**, 636 (1991).
[20] J. M. Soto-Crespo, E. M. Wright, and N. N. Akhmediev, Phys. Rev. A **45**, 3168 (1992).

[21] F. Vidal and T. W. Johnston, Phys. Rev. Lett. **77**, 1282 (1996).
[22] J. H. Marburger and E. Dawes, Phys. Rev. Lett. **21**, 556 (1968); Phys. Rev. **179**, 862 (1969).
[23] V. E. Zakharov, V. V. Sobolev, and V. C. Synackh, Zh. Éksp. Teor. Fiz. **60**, 136 (1971) [Sov. Phys. JETP **33**, 77 (1971)].
[24] V. M. Malkin, Physica D **64**, 251 (1993).
[25] J. F. Lam, B. Lippmann, and F. Tappert, Phys. Fluids **20**, 1176 (1977).
[26] N. G. Vakhitov and A. A. Kolokolov, Izv. Vyssh. Uchebn. Zavect. Radiofiz. **16**, 1020 (1973) [Sov. Radiophys. **16**, 783 (1975)]; A. A. Kolokolov, *ibid.* **17**, 1332 (1974) [*ibid.* **17**, 1016 (1976)].
[27] D. Anderson and M. Bonnedal, Phys. Fluids **22**, 105 (1979).
[28] D. Anderson, Phys. Rev. A **27**, 3135 (1983).
[29] *Handbook of Mathematical Functions*, edited by M. Abramowitz and I. A. Stegun (Dover, New York, 1970), p. 1004.
[30] C. Cohen-Tannoudji, B. Diu, and F. Laloë, *Mécanique Quantique* (Hermann, Paris, 1977), p. 412.
[31] C. Cohen-Tannoudji, B. Diu, and F. Laloë, *Mécanique Quantique* (Ref. [30]), p. 1292.
[32] C. Cohen-Tannoudji, B. Diu, and F. Laloë, *Mécanique Quantique* (Ref. [30]), p. 78.
[33] J. P. Gordon, J. Opt. Soc. Am. B **9**, 91 (1992).